Tracking Cooper Pairs in a Cuprate Superconductor by Ultrafast Angle-Resolved Photoemission

Christopher L. Smallwood,[1,2] James P. Hinton,[1,2] Christopher Jozwiak,[3] Wentao Zhang,[2] Jake D. Koralek,[2] Hiroshi Eisaki,[4] Dung-Hai Lee,[1,2] Joseph Orenstein,[1,2] Alessandra Lanzara[1,2]*

In high-temperature superconductivity, the process that leads to the formation of Cooper pairs, the fundamental charge carriers in any superconductor, remains mysterious. We used a femtosecond laser pump pulse to perturb superconducting $Bi_2Sr_2CaCu_2O_{8+\delta}$ and studied subsequent dynamics using time- and angle-resolved photoemission and infrared reflectivity probes. Gap and quasiparticle population dynamics revealed marked dependencies on both excitation density and crystal momentum. Close to the *d*-wave nodes, the superconducting gap was sensitive to the pump intensity, and Cooper pairs recombined slowly. Far from the nodes, pumping affected the gap only weakly, and recombination processes were faster. These results demonstrate a new window into the dynamical processes that govern quasiparticle recombination and gap formation in cuprates.

The lifetime of Bogoliubov quasiparticles, the low-energy excitations of a superconductor, contains a wealth of information pertinent to the origin of superconductivity in a given material (*1*). This lifetime reflects two distinct processes: quasiparticle scattering and recombination. In the former, a quasiparticle scatters from one momentum state to another, conserving the fermionic particle number. Recombination, by contrast, refers to interactions in which two quasiparticles annihilate. To conserve energy and momentum, recombination must involve emission of other excitations—for example, phonons or magnons—to which the quasiparticles are strongly coupled. Measurement of quasiparticle recombination rates as a function of their energy and momentum can, in principle, provide direct information about the interactions that induce Cooper pairing and superconductivity (*2*). Only recently, with the demonstration that angle-resolved photoemission spectroscopy (ARPES) can be performed with ultrashort laser pulse sources (*3*–*9*), have measurements with the necessary energy, momentum, and time resolution become possible. We present the results of experiments that use synchronized laser pulses to perform time-resolved ARPES measurements of quasiparticle recombination and gap dynamics in the high-temperature superconductor $Bi_2Sr_2CaCu_2O_{8+\delta}$.

Measurements were performed at 18 K on an optimally doped sample with a critical temperature (T_c) of 91 K. A transient state is created with an infrared laser pump pulse ($h\nu$ = 1.48 eV, where $\hbar$ is Planck's constant and ν is the photon frequency). and measured via photoemission shortly thereafter, with a temporal resolution of 300 fs, using an ultraviolet probe pulse ($h\nu$ = 5.9 eV). The experiment benefits from high momentum and energy resolution (0.003 $Å^{-1}$ and 23 meV, respectively) and the ability to explore low pump fluences (2 to 15 $\mu J/cm^2$).

Figure 1 shows typical equilibrium and transient ARPES dispersions (t = −1 and 0.6 ps, respectively) for cuts along nodal and off-nodal directions in k-space. Here, the time origin t = 0 coincides with the application of the pump pulse. The off-nodal cut has an equilibrium gap of 15 meV. In both cuts, a well-defined kink [marked by arrows in (A), (B), (F), and (G)] (*10*, *11*) separates sharply defined coherent dispersive features

[1]Department of Physics, University of California, Berkeley, CA 94720, USA. [2]Materials Sciences Division, Lawrence Berkeley National Laboratory, Berkeley, CA 94720, USA. [3]Advanced Light Source, Lawrence Berkeley National Laboratory, Berkeley, CA 94720, USA. [4]Electronics and Photonics Research Institute, National Institute of Advanced Industrial Science and Technology, Ibaraki 305-8568, Japan.

*To whom correspondence should be addressed. E-mail: alanzara@lbl.gov

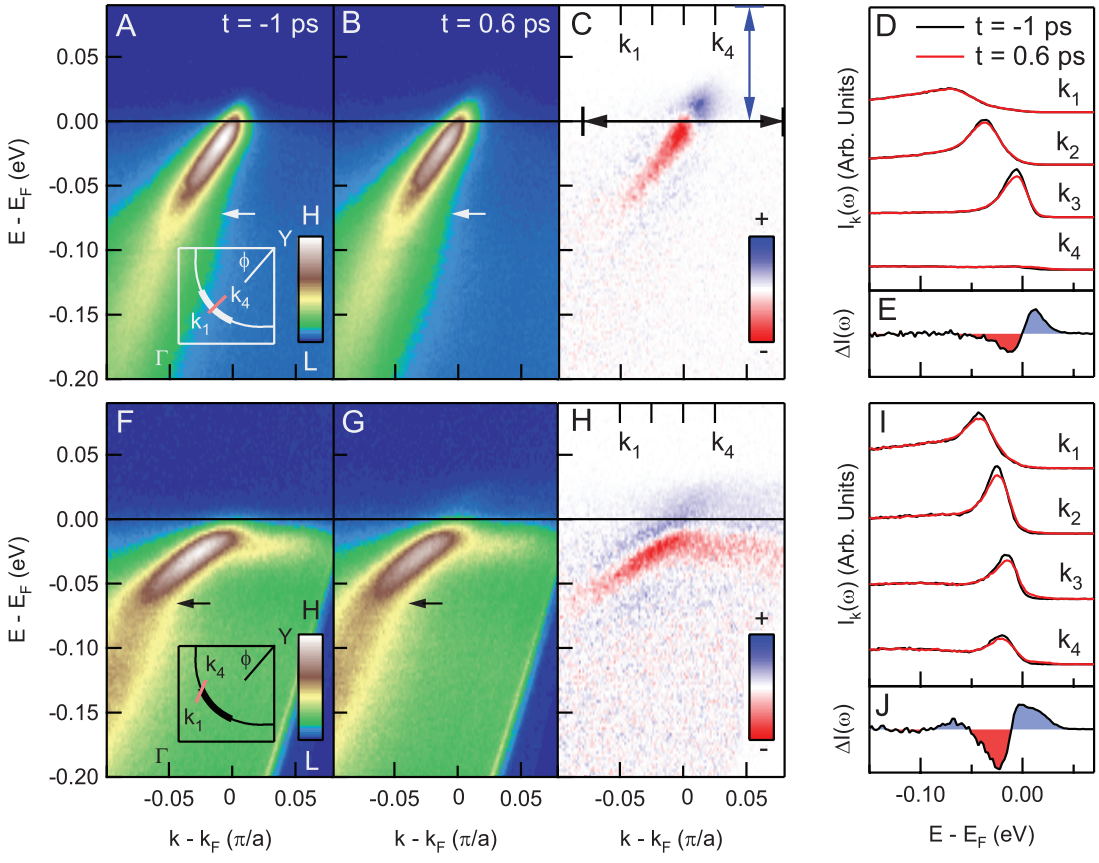

Fig. 1. Typical ARPES dispersions before and after pumping for nodal (ϕ = 45°) and gapped (ϕ = 31°) regions of k-space. The incident pump fluence was 5 $\mu J/cm^2$. (**A**) Equilibrium (t = −1 ps) and (**B**) transient (t = 0.6 ps) energy-momentum maps for the nodal state. Data are shown with identical color scales. The inset shows the location of the cut. The arrow marks the position of the dispersion kink. (**C**) Subtraction between (A) and (B). Blue indicates intensity gain and red intensity loss. (**D**) Energy distribution curves (EDCs) from k_1 to k_4 for equilibrium (in black) and transient (in red) states. EDCs are shifted vertically for ease of comparison. (**E**) Difference between transient and equilibrium EDCs, integrated across the double black arrow in (C). (**F** to **J**) Same as (A to E) but for a gapped (off-nodal) momentum cut. Spectra have been corrected for detector nonlinearity. The diagonal line in the lower right portion of (F) and (G) is the edge of the detector.

from poorly defined incoherent features, as is also visible in the selected energy distribution curves (EDCs) shown in (D) and (I). The following changes are evident in the transient spectra: (i) a decrease in intensity below the Fermi level (E_F) and slight broadening in the coherent spectra [(C to E) and (H to J)], similar to a previous report for nodal quasiparticles (*5*) and mainly confined below the kink binding energies (*10*, *11*); (ii) an overall transfer of spectral weight across E_F [(C), (E), (H), and (J)], indicating the creation of transient quasiparticles; and (iii) a small shift of the spectral peak toward E_F in the off-nodal cut [(H and (I)], indicating a partial closure of the superconducting gap.

Figure 2 shows the temporal evolution of the superconducting gap in response to photoexcitation, as extracted from symmetrized EDCs at k_F, the Fermi wave vector (*12*). Panels (A and B) and (C and D) correspond to two representative cuts at $\phi = 32°$ and $\phi = 27°$, respectively, with ϕ defined according to the inset of (E). These spectra indicate very different responses of the gap amplitude to photoexcitation for the two cuts. The gap is relatively insensitive to fluences below 5 μJ/cm^2, but a fluence of 13 μJ/cm^2 induces a clear reduction in size. As shown in (E), the gap closer to the node decreases by 55% of its equilibrium magnitude, whereas the gap at $\phi = 27°$ decreases by only 20%. This may indicate different dynamics inside and outside the Fermi arc, which is reported to end rather abruptly at $\phi = 30°$ for samples of this doping (*13*, *14*), although studies farther from the node are needed. Gap recovery rates are illustrated in Fig. 2F, where the curves from (E) have been inverted and rescaled by their maximum change. The initial recovery rate is slower for states closer to the node (0.9 ± 0.6 ps^{-1}) than for states farther from the node

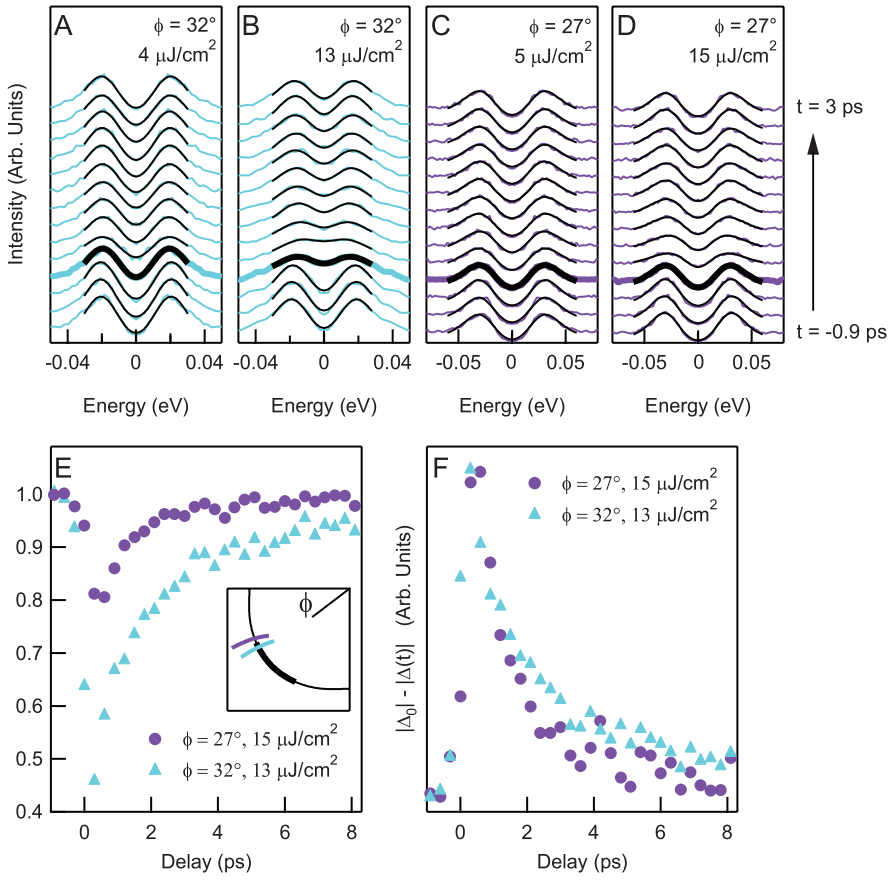

Fig. 2. Evolution of the superconducting gap after pump excitation. Symmetrized EDCs at k_F for $\phi = 32°$ at low (**A**) and higher (**B**) fluence. The gap is obtained by fitting to a phenomenological model (*12*), but can be approximated by halving the distance between positive and negative peaks. Bold curves correspond to $t = 0$. For additional gap fitting details, see supplementary materials (*15*). (**C** and **D**) Analogous EDCs for a cut at $\phi = 27°$. (**E**) Gap magnitude normalized by its equilibrium value versus pump-probe delay for momentum cuts at $\phi = 27°$ and $\phi = 32°$. (**F**) Gap magnitude, inverted and normalized by maximal change upon pumping in order to compare recovery rates.

Fig. 3. Quasiparticle recombination dynamics versus pump fluence and crystal momentum. ARPES data correspond to intensity change above E_F (ΔI) as integrated between the blue and black double arrows in Fig. 1C. Time-resolved reflectivity rates correspond to fractional change in reflectivity. (**A**) Nodal decay curves at 2, 5, and 10 μJ/cm^2, normalized to the same amplitude. (**B**) Analogous off-nodal decay curves ($\phi = 31°$). (**C**) Overlay of nodal and off-nodal curves at the same fluence. (**D**) Initial decay rate γ_0 versus fluence, obtained by fitting decay curves at short times [for $\Delta I\ (t) \gtrsim \Delta I_0/2$] to the convolution of a Gaussian and the function $f(t) = \Delta I_0 e^{-\gamma_0(t-t_0)}\Theta(t - t_0)$, where ΔI_0 and t_0 are additional fit parameters. Time-resolved reflectivity rates were multiplied by 3/2 in order to take the finite penetration depth of the optical probe into account (*15*).

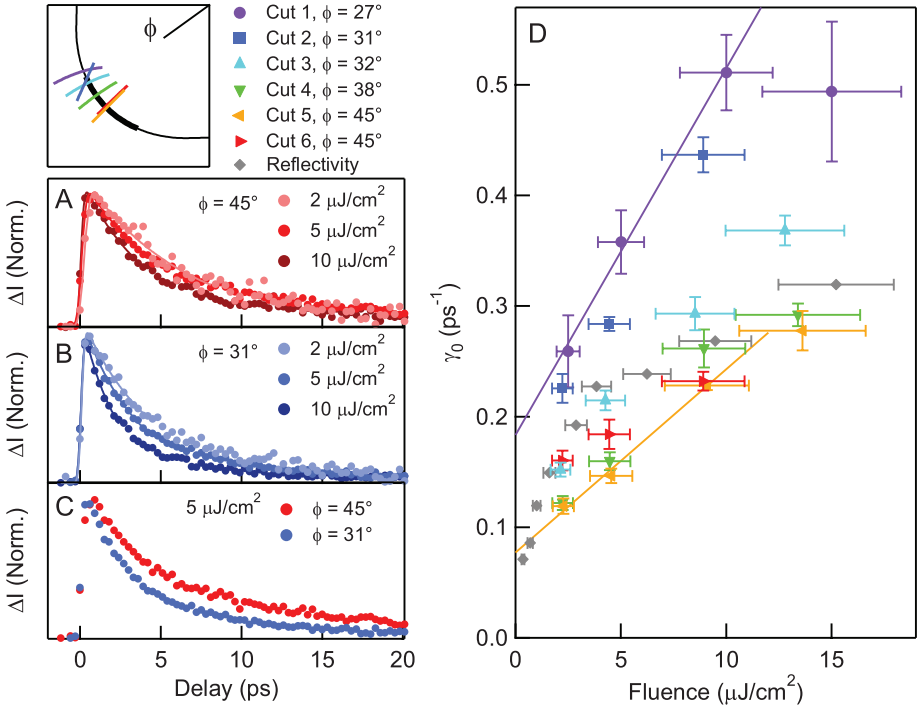

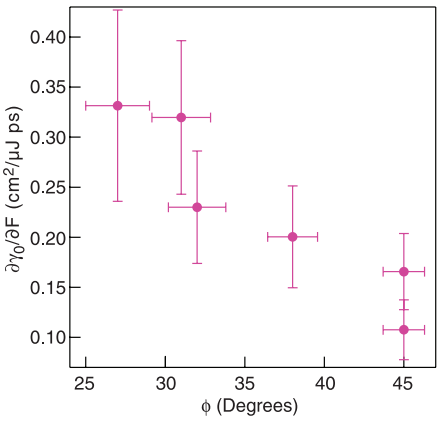

Fig. 4. Initial rate of increase $\partial\gamma_0/\partial F$ as extracted from straight line fits to the data in Fig. 3D for fluence $F < 12$ μJ/cm^2. The horizontal axis corresponds to the Fermi surface angle.

(1.3 ± 0.6 ps^{-1}), although the contrast is less apparent than that between amplitudes.

Figures 3 and 4 show quasiparticle recombination dynamics. In this low-fluence regime, the gap is almost unchanged for most of the recovery process, so quasiparticle recombination is largely decoupled from gap dynamics. Figure 3, A to C, shows the temporal evolution of the above-E_F spectral change ΔI for representative nodal and off-nodal k-space cuts, where ΔI is defined by the integrated intensity change across the blue and black double arrows in Fig. 1C. The spectral change is nearly symmetric above and below E_F in this fluence regime, so we focus on the intensity above E_F because of its superior statistics and smaller background. Faster decay rates occur at higher fluences and off-nodal momenta, an effect that cannot be explained by equilibrium heating (*15*).

Figure 3D summarizes the dependence of quasiparticle recombination on fluence and momentum. The rate γ_0 is defined by fitting the decay curves at short times to the convolution of a Gaussian and decaying exponential (*16*, *17*). In line with Fig. 3, A to C, two prominent decay rate trends are apparent: (i) fluence dependence, with faster initial decay rates γ_0 occurring at higher fluences; and (ii) momentum dependence, with off-nodal decay rates increasing faster with fluence than those at the node. The first trend implies that intrinsic quasiparticle recombination processes are observed (*17*, *18*). The second trend indicates that this recombination occurs more rapidly in off-nodal regions of k-space than at the node. The fluence dependence is also complementary to ultrafast studies using all-optical techniques, which report a marked dependence of decay rate on fluence, particularly in the low-fluence regime (*16*–*20*), and there is overall agreement between the ARPES results and a time-resolved reflectivity measurement taken on the same sample (gray circles in Fig. 3D). The decay rate measured by reflectivity is uniformly faster than nodal ARPES decay rates (cuts 5 and 6), but slower than the off-nodal rates (cuts 1 to 3), suggesting that optical spectroscopy provides an effective momentum-integrated average of the quasiparticle population. Notably, along both $\phi = 27°$ and 32° directions, quasiparticle decay rates are slower than the gap recovery rates in Fig. 2: Compare 1.3 ± 0.4 ps^{-1} and 0.9 ± 0.6 ps^{-1} for the gap recovery versus 0.49 ± 0.06 ps^{-1} and 0.37 ± 0.01 ps^{-1} for the intensity recovery. This indicates that the superconducting gap recovers well before the nonequilibrium quasiparticle population drops to zero. A potentially related effect occurs at equilibrium in the Bardeen, Cooper, and Schrieffer (BCS) model, where the gap becomes large for T only slightly below T_c. Finally, the fluence and momentum dependencies reported here contrast with the findings of another time-resolved ARPES work (*6*), in which the quasiparticle recombination rate was reported to be independent of both fluence and momentum. The discrepancy might be explained by the higher fluences used in the previous work, which likely result in a complete closure of the superconducting gap, or by the coarser momentum and energy resolution compared to the present study.

As noted above [see also supplementary materials (*15*)], the fluence dependence of γ_0 means that ARPES decay rates are connected to intrinsic quasiparticle recombination processes. Time-resolved optical measurements indicate that the total (momentum-integrated) population of photoexcited quasiparticles $n_{ex}(t)$ can be described by a bimolecular rate equation (*17*, *18*),

$$\frac{\dot{n}_{ex}}{n_{ex}} = -R(n_{ex} + 2n_T) \qquad (1)$$

where R is a quasiparticle recombination constant, and n_T is the population of thermal quasiparticles. This is a special case of the Rothwarf-Taylor model of quasiparticle recombination (*21*), which has been successfully used to model dynamics of both conventional and high-temperature superconductors (*17*–*20*, *22*–*28*). The general model also incorporates negative feedback from "hot" bosons ($\hbar\omega \gtrsim 2\Delta$) that are created by the quasiparticle decay process. For low fluence and temperature the model reduces to Eq. 1 under both weak feedback and strong feedback (boson bottleneck) scenarios, which produce differing interpretations of the coefficient R (*17*, *23*). In both approximations, bimolecular recombination is the active ingredient in fluence-dependent dynamics.

In contrast to time-resolved optics, ARPES measures the momentum-dependent nonequilibrium quasiparticle density $n_k(t)$. The short-time fluence-dependent recombination dynamics are given by

$$\frac{\dot{n}_k}{n_k} \approx -\int R_{kk'} n_{k'} d^2k' \qquad (2)$$

where $R_{kk'}$ is a modified recombination coefficient for the interaction between quasiparticles at specific points k and k' in reciprocal space. A weighted average of $R_{kk'}$ over k' is given by $\partial\gamma_0/\partial F$, the rate of increase of the initial decay rate γ_0 with fluence (*15*). Figure 4 shows an analysis of $\partial\gamma_0/\partial F$ as calculated by fitting straight lines to the data in Fig. 3D for fluences $F < 12$ μJ/cm^2. It is clear that $\partial\gamma_0/\partial F$ increases with decreasing Fermi surface angle ϕ, which means that the rate of recombination is enhanced as the quasiparticle momentum moves farther from the node.

One potential scenario for the momentum dependence of the recombination rates is that with increasing distance from the node, the quasiparticle energy and momentum approach resonance with charge or spin density wave fluctuations to which the electrons are strongly coupled. For example, a prominent neutron spin resonance is observed in $Bi_2Sr_2CaCu_2O_{8+\delta}$ along the (1,1) momentum vector (*29*). Resonance between this mode and a quasiparticle pair would occur at a Fermi surface angle of about 12°, leading to the prediction of a peak in $\partial\gamma_0/\partial F$ at this Fermi surface angle. We believe that demonstrating that recombination can be mapped using time-resolved ARPES, and observing its strong momentum dependence, will further stimulate development of pulsed sources that are capable of reaching all the relevant regions of momentum space.

References and Notes

1. J. R. Schrieffer, *Theory of Superconductivity* (Westview, Boulder, CO, 1999).
2. S. B. Kaplan *et al.*, *Phys. Rev. B* **14**, 4854 (1976).
3. L. Perfetti *et al.*, *Phys. Rev. Lett.* **99**, 197001 (2007).
4. F. Schmitt *et al.*, *Science* **321**, 1649 (2008).
5. J. Graf *et al.*, *Nat. Phys.* **7**, 805 (2011).
6. R. Cortés *et al.*, *Phys. Rev. Lett.* **107**, 097002 (2011).
7. T. Rohwer *et al.*, *Nature* **471**, 490 (2011).
8. J. C. Petersen *et al.*, *Phys. Rev. Lett.* **107**, 177402 (2011).
9. L. Rettig *et al.*, *Phys. Rev. Lett.* **108**, 097002 (2012).
10. A. Lanzara *et al.*, *Nature* **412**, 510 (2001).
11. T. Cuk *et al.*, *Phys. Rev. Lett.* **93**, 117003 (2004).
12. M. R. Norman, M. Randeria, H. Ding, J. C. Campuzano, *Phys. Rev. B* **57**, R11093 (1998).
13. K. Tanaka *et al.*, *Science* **314**, 1910 (2006).
14. W. S. Lee *et al.*, *Nature* **450**, 81 (2007).
15. Supplementary materials and methods are available on *Science* Online.
16. G. P. Segre *et al.*, *Phys. Rev. Lett.* **88**, 137001 (2002).
17. N. Gedik *et al.*, *Phys. Rev. B* **70**, 014504 (2004).
18. R. A. Kaindl, M. A. Carnahan, D. S. Chemla, S. Oh, J. N. Eckstein, *Phys. Rev. B* **72**, 060510 (2005).
19. N. Gedik *et al.*, *Phys. Rev. Lett.* **95**, 117005 (2005).
20. G. Coslovich *et al.*, *Phys. Rev. B* **83**, 064519 (2011).
21. A. Rothwarf, B. N. Taylor, *Phys. Rev. Lett.* **19**, 27 (1967).
22. J. Demsar *et al.*, *Phys. Rev. Lett.* **91**, 267002 (2003).
23. V. V. Kabanov, J. Demsar, D. Mihailovic, *Phys. Rev. Lett.* **95**, 147002 (2005).
24. P. Kusar *et al.*, *Phys. Rev. Lett.* **101**, 227001 (2008).
25. C. Giannetti *et al.*, *Phys. Rev. B* **79**, 224502 (2009).
26. D. H. Torchinsky, G. F. Chen, J. L. Luo, N. L. Wang, N. Gedik, *Phys. Rev. Lett.* **105**, 027005 (2010).
27. D. H. Torchinsky *et al.*, *Phys. Rev. B* **84**, 104518 (2011).
28. M. Beck *et al.*, *Phys. Rev. Lett.* **107**, 177007 (2011).
29. H. F. Fong *et al.*, *Nature* **398**, 588 (1999).

Acknowledgments: We thank R. A. Kaindl, D. A. Siegel, S. D. Lounis, T. Miller, and R. Johnson for useful discussions. This work was supported by the Director, Office of Science, Office of Basic Energy Sciences, Materials Sciences and Engineering Division, of the U.S. Department of Energy under Contract No. DE-AC02-05CH11231.

Supplementary Materials

www.sciencemag.org/cgi/content/full/336/6085/1137/DC1
Materials and Methods
Supplementary Text
Figs. S1 to S5
References (*30*–*35*)

5 December 2011; accepted 10 April 2012
10.1126/science.1217423

Tracking Cooper Pairs in a Cuprate Superconductor by Ultrafast Angle-Resolved Photoemission

Christopher L. Smallwood *et al.*

Science **336**, 1137 (2012);
DOI: 10.1126/science.1217423

Science (print ISSN 0036-8075; online ISSN 1095-9203) is published weekly, except the last week in December, by the American Association for the Advancement of Science, 1200 New York Avenue NW, Washington, DC 20005.